Word count: 8,922

Revision 2

Measuring H_2O Concentrations in Olivine by Secondary Ion Mass Spectrometry: Challenges and Paths Forward

Authors

W. Henry Towbin[a 1], Terry Plank[a], Emily Klein[b], Erik Hauri[c 2]

Affiliations

[a] Lamont-Doherty Earth Observatory, Columbia University, 61 Route 9W, PO Box 1000, Palisades, NY, 10964, USA

[b] Earth and Climate Sciences Division, Nicholas School of the Environment, Duke University, Durham, NC, 27708

[c] Department of Terrestrial Magnetism, Carnegie Institution for Science, 5241 Broad Branch Road, N.W., Washington, D.C., 20015, US

[1] Corresponding Author: henry.towbin@ldeo.columbia.edu

[2] Deceased September 5, 2018. Dr. Erik Hauri collected the new data presented here and performed preliminary data reductions, but did not participate in the writing of this manuscript. Our analysis was guided by our personal communications with him in January of 2018.

This is the peer-reviewed, final accepted version for American Mineralogist, published by the Mineralogical Society of America.
The published version is subject to change. Cite as Authors (Year) Title. American Mineralogist, in press.
DOI: https://doi.org/10.2138/am-2022-8247. http://www.minsocam.org/

Abstract

Trace concentrations of H_2O in olivine strongly affect diverse mantle and magmatic processes. H_2O in olivine has been difficult to accurately quantify due to challenges in sample preparation and measurement, as well as significant uncertainties in standard calibrations. Here we directly compare secondary-ion mass spectrometry (SIMS) measurements of the olivine standards of Bell et al. (2003, hereafter Bell03) and Withers et al. (2012, hereafter Withers12) upon which most SIMS and Fourier transform infrared (FTIR) spectroscopy analyses are based. In the same SIMS session, we find that the olivine standards from the two studies are offset by ~50%, forming lines of different slope when comparing SIMS measurements to the independent nuclear reaction analysis (NRA) in Bell03 and elastic recoil detection analysis (ERDA) in Withers12. This offset is similar to the ~40% offset that exists in the FTIR absorption coefficients determined by those two same studies, and points to the NRA-ERDA data as the cause for the offset more than different IR absorption characteristics of the different olivines. We find that the Withers 12 olivine standards form the most precise calibration line, and that the measured Bell03 olivine standards have issues of reproducibility and accuracy due to the presence of hydrous inclusions (as documented previously by Mosenfelder et al., 2011). Owing to the limited availability of the Withers12 olivine standards, however, we recommend using orthopyroxene standards (Kumamoto et al., 2017) to calibrate H_2O in olivine by SIMS due to similar calibration slopes. We revise the reference values of current orthopyroxene standards to account for uncertainties in the Bell et al. (1995) manometry data. With these revised values, the orthopyroxene calibration line is within 12% of the Withers12 olivine line, which is within the long-term uncertainty of the SIMS olivine measurements. We apply our SIMS calibration protocol to revise estimates of the

partition coefficients for H_2O between olivine and melt, resulting in a value of 0.0009 +/- 0.0003 at pressures ~0.2 - 2 GPa. This brings into closer agreement the partition coefficients determined from experimental studies with those based on natural studies of olivine-hosted melt inclusions.

INTRODUCTION

The presence of hydrogen in nominally anhydrous minerals (NAMs) is known to influence a wide range of mantle and magmatic processes (e.g., Bell and Rossman, 1992). The solidus of mantle peridotite, for example, varies markedly as a function of the hydrogen concentration in NAMs, which in turn governs the extent and pressure of mantle melting (e.g., Gaetani and Grove, 1998; Hirschmann et al., 1999; Sarafian et al., 2017). It should be noted that hydrogen bonded to oxygen in mineral structures is often measured as H or OH and reported as H_2O ppm (μg/g), with some studies colloquially using the term "water". Here we use H_2O to refer to the concentration of structurally bound H in a crystal, and where appropriate, H^+ for discussing the diffusing species. Olivine typically has only trace concentrations of H_2O (0-60 ppm), yet because it is the dominant upper-mantle mineral, it plays a prominent role in mantle dynamics (Demouchy & Bolfan-Casanova, 2016). Rheological studies show, for example, that olivine's strength may be reduced by up to an order of magnitude with as little as tens of ppm of H_2O (Faul et al. 2016), with profound effects on mantle viscosity and dynamics (Hirth and Kohlstedt, 1996). The H_2O concentration in olivine is also predicted to be a determining factor in the electrical conductivity of the mantle (Gardés et al., 2017), which is used for geophysical modeling of mantle structure (e.g., Naif et al., 2013). Furthermore, the rates and dynamics of magma ascent are often constrained by studying diffusion-induced concentration profiles of H_2O

in magmatic and mantle olivine. (Demouchy et al., 2006; Peslier and Luhr, 2006; Ferris et al. 2016; Newcombe et al. 2020).

Despite recent advances in the measurement and quantification of H_2O in olivine, there remain a number of challenges. Some of these challenges arise from difficulties inherent to the analytical techniques used, while others arise from disagreements and uncertainties on the reference concentrations of calibration standards. In addition, as analytical methods have evolved, earlier measurements cannot easily be compared with those performed according to today's best practices. Many of these issues have been reviewed by Demouchy and Bolfan-Casanova (2016). Additionally, Mosenfelder et al. (2011) provided a thorough review of challenges specific to secondary ion mass spectrometry (SIMS) calibrations of H_2O concentration in olivine.

Prompted by the known challenges in measuring the concentration of H_2O in olivine and other NAMs, we collected a comprehensive SIMS dataset to directly address a number of the vexing problems. Here we present these new data and compare them with previous findings to advance approaches for quantifying H_2O concentrations in NAMs by SIMS. Specifically, we directly compare the two most widely used sets of standard reference materials (hereafter "standards") for measuring H_2O concentrations in olivine: those of Bell03 and Withers12. This is critical, as these standards produce results that differ from one another by 37%. Based on our new data and analyses, we demonstrate the difficulties in using the existing Bell03 olivine standards and argue for an alternative calibration involving the publicly available orthopyroxene standards (Kumamoto et al., 2017). In addition, we apply this calibration approach to resolve discrepancies in published partition coefficients for H_2O in olivine and basaltic melts.

This is the peer-reviewed, final accepted version for American Mineralogist, published by the Mineralogical Society of America.
The published version is subject to change. Cite as Authors (Year) Title. American Mineralogist, in press.
DOI: https://doi.org/10.2138/am-2022-8247. http://www.minsocam.org/

CHALLENGES OF MEASURING H_2O IN OLIVINE

The two most widely used methods for measuring H_2O concentrations in olivine and other NAMs are SIMS and Fourier transform infrared spectroscopy (FTIR). While each method can produce reliable results, each has unique challenges for the measurement of NAMs that we outline here.

Pros and Cons of FTIR and SIMS measurements

FTIR analysis of olivine involves the measurement of the absorbance of IR-radiation due to OH-bond stretching, which is then converted to concentration using molar absorptivity coefficients and the Beer-Lambert-Bouguer Law (Beer, 1852; Paterson, 1982). Compared to most other methods, FTIR has the lowest detection limit for quantifying H_2O concentrations in olivine for thick (> 1 mm) specimens. It is also non-destructive, inexpensive, producing rapid analyses and sample maps without challenging instrumentation calibration. It has the additional benefit of providing information on the bonding environment of the hydrogen in the olivine structure (e.g., Berry et al., 2005, 2007).

There are several limitations to the measurement of H_2O concentrations in NAMs by FTIR, however, the first of which relates to sample size and preparation requirements. Infrared-absorbance is measured along an integrated path through the crystal and not at a limited near surface volume. Therefore, samples must be polished on two co-planar surfaces and placed within the IR beam for transmission measurements. Samples must be relatively thick (> 50μm) for measurements at low H_2O concentrations (<10 ppm). Second, the IR absorbance in olivine is anisotropic, so grains must be carefully oriented along their crystallographic axes, or measured in multiple grains from the same population in random orientation (e.g., Asimow et al., 2006). Third, IR-absorbances are challenging to determine from FTIR spectra. Each spectrum has a

baseline that must be subtracted in order to measure peak heights or areas. Identification of baselines is subjective, and can vary between grains and along profiles measured across single grains. Indeed, there is no accepted procedure for subtracting the baseline under OH peaks in NAMs. Fourth, while a benefit of FTIR is that spectra provide information on the bonding environment of hydrogen it can be difficult to deconvolve the various OH peaks in the spectrum, thus the added information comes with additional complexity. For example, it is unclear if a single molar absorptivity coefficient can be applied to different OH peaks as several studies have argued for a wavenumber-dependence (Paterson,1982; Libowitsky and Rossman, 1997; Balan et al., 2011; Blanchard et al., 2016, Tollan et al., 2017; Jollands et al. 2021). Wavenumber-dependence might not be apparent in the Bell03 and Withers12 studies, however, because both studies measured samples with a similar distribution of peaks in the OH-stretching region of their FTIR spectra.

SIMS analysis has the benefit of measuring an area at the surface, in contrast to the integrated beam path of FTIR, which makes it possible to analyze grains too small to doubly polish for FTIR. It also provides a direct measure of total H_2O concentration irrespective of bonding site. Specifically, SIMS measures hydrogen ions directly (typically either ^{1}H or $^{16}O^{1}H$), in contrast to FTIR which measures IR-absorbance due to OH-bond stretching. While it lacks information on bonding sites, the SIMS signal has the benefit of being simpler to interpret compared to FTIR, in view of the latter's spectral processing complexities. One major drawback of SIMS is its extreme sensitivity to sample contamination. Samples must be rigorously cleaned in several solvents to remove any surface organic, plastic or oil compounds, and baked in vacuum ovens before mounting. For these reasons, the preferred mounting medium is indium metal (Hauri et al., 2002; Koga et al., 2003) and not the more common and easily prepared epoxy

This is the peer-reviewed, final accepted version for American Mineralogist, published by the Mineralogical Society of America.
The published version is subject to change. Cite as Authors (Year) Title. American Mineralogist, in press.
DOI: https://doi.org/10.2138/am-2022-8247. http://www.minsocam.org/

or resin. In addition, the SIMS instrument itself must be "baked" to remove contamination from the vacuum chamber, because hydrogen released from these contaminants can lead to a changing background signal. Changes in the ion beam or the charge-compensating electron beam can also lead to variations in instrument sensitivity that must be quantified with drift standards. Finally, instruments must be optimized to achieve detection limits on the order of < 10 ppm H_2O, necessary to produce precise measurements of H_2O in many natural NAMs, particularly olivine that often has H-loss profiles that approach 0 ppm H2O at the rims.

Calibration of FTIR and SIMS measurements and associated complications

Both SIMS and FTIR depend upon calibration to standards developed by independent and more laborious methods. Two such methods, nuclear reaction analysis (NRA) and elastic recoil detection analysis (ERDA), have provided absolute concentrations of hydrogen in a sample without requiring matrix-matched standardization (e.g. NRA: Endisch et al., 1994; ERDA: Bureau et al., 2009). In addition to calibrating to such independently validated standards, SIMS analyses are often calibrated to standards measured by FTIR, using absorption coefficients that have also been determined from NRA or ERDA data. Thus, the accuracy of FTIR molar absorptivity coefficients for H_2O in NAMs plays a key role in the accuracy of many SIMS calibrations for such samples.

For measuring H_2O concentrations in olivine, two widely cited studies produced independent calibrations to determine the FTIR-absorbance coefficients. Bell03 used NRA to independently measure the H_2O concentrations in natural olivine samples; Withers12 measured synthetic olivine samples by ERDA. These studies, however, provide FTIR molar absorptivity coefficients, for calculating H_2O concentrations from OH-peak absorbances, that differ by 37±5%. Partially because of the discrepancy between the Bell and Withers FTIR calibrations, the

157 petrological community has not settled on a common calibration approach for quantifying H_2O
158 concentrations in olivine. The Bell03 method, based on NRA, has two main advantages: the
159 standards include natural olivines with H_2O concentrations relevant for magmatic systems (16 –
160 220 ppm by weight), and NRA has low detection limits (10-20 ppm; Endisch et al., 1994) The
161 FTIR spectra of the Bell03 olivines are typical of most natural olivine (Demouchy and Bolfan-
162 Casanova, 2016**)**. On the other hand, the Withers12 study measured seven synthetic Fo ~90
163 olivines, with concentrations between 300 and 2000 ppm, based on ERDA, which has higher
164 detection limits (50-100 ppm; Bureau et al., 2009). Typical natural olivines, however, rarely have
165 concentrations greater than ~50 ppm (Demouchy and Bolfan-Casanova, 2016) so it is unclear if
166 the H_2O-rich Withers12 olivines can be used to accurately calibrate natural ones. Nevertheless,
167 ERDA has some advantages over NRA. While both NRA and ERDA have sampling depths of 2
168 μm, the ERDA measurements of Withers12 had a significantly smaller beam footprint (4μm x
169 16μm) than typical NRA beam sizes (hundreds of μm to a few mm in diameter). The smaller
170 volume analyzed allows ERDA users to map the sample surface and thus identify sample
171 heterogeneity and avoid surface contamination.

172 Although the Bell03 olivines have been used extensively as SIMS standards, they are
173 known to be heterogeneous. Mosenfelder et al. (2011) found that the two samples with the
174 highest H_2O concentrations measured by Bell03, GRR1012 and KLV23, contain hydrous non-
175 olivine defects and fluid inclusions, and thus they recommended discontinuing use of KLV-23 as
176 a standard and continuing use of GRR1012 only with careful screening for heterogenous
177 measurements. This finding is consistent with Bell03 reporting IR-peaks (~3700 cm^{-1}) thought to
178 be indicative of hydrous non-olivine inclusions in these standards (Mosenfelder et al., 2011). It is
179 unknown how much the FTIR and NRA measurements are influenced by these hydrous

inclusions, but it is possible that they contribute to the higher IR-calibration coefficient reported by Bell03. Because NRA, unlike ERDA, is unable to distinguish between olivine and hydrous inclusions it calls into question the accuracy of the Bell03 measurements, particularly because the Bell03 calibration coefficients produce higher concentrations that those of Withers12. While the Withers12 standards have higher concentrations of H_2O than natural olivines, their homogeneity, as measured by ERDA, FTIR and SIMS, make them inherently better standards for calibration of SIMS analyses. Some recent studies advocate for either the Bell03 or Withers12 FTIR calibrations based on which they think is most suitable for their analysis, while others simply cite concentrations determined with both (e.g. Padrón-Navarta et al., 2014, Ferriss et al., 2018; Tollan et al., 2017; Jollands et al., 2019; Jollands et al., 2021). Here we mainly focus on comparison of hydrogen concentration in the Bell and Withers samples as measured by SIMS so as to avoid the complexities introduced by different OH point-defects that influence FTIR calibration coefficients. FTIR is uniquely sensitive to the OH-bonding environment, and therefore differences in the trace elements of the Bell03 and Wither12 standards could affect the IR spectra in ways that are difficult to quantify. SIMS is much less sensitive to OH-bonding environment and allows us to directly compare hydrogen concentrations determined by both NRA and ERDA.

The Carnegie Sessions

In June of 2017, olivine standards from Withers12 were analyzed using the Cameca NanoSIMS 50L at the Carnegie Institution for Science. This analytical session is notable given that all of the Withers12 standards were measured together with standards from both Bell03 and Bell et al. (2004). This enables us to investigate whether the SIMS calibration based on

Withers12 ERDA data or one based on Bell03 NRA data, is more precise. In addition, during June 2017 and August 2016, a large set of orthopyroxene and clinopyroxene standards reported by Kumamoto et al. (2017) were measured by NanoSIMS together with the set of pyroxenes that had been measured at Carnegie for over a decade (Koga et al., 2003; Aubaud et al., 2004; Wade et al., 2008; Lloyd et al. 2016; Newcombe et al., 2020). We have also included a supplemental compilation of NAMS and basaltic glass standards measured repeatedly on the Carnegie Cameca 6F SIMS from 2007 to 2019. Taken together, these analyses offer the opportunity for intercomparison of one of the most extensive sets of NAMs standards measured by SIMS, thus providing unique insights to guide further calibrations.

METHODS

In preparation for analysis by SIMS, polished standard reference olivines and pyroxenes were mounted in indium and placed under vacuum for several days. The Carnegie Cameca NanoSIMS 50L is able to achieve extremely low blanks (1-2 ppm H_2O) due to extensive baking procedures and using indium sample mounts, which do not out-gas under vacuum, rather than epoxy. Analytical protocols are similar to those reported by Kumamoto et al. (2017) and Newcombe et al. (2020). H_2O was measured as $^{16}O^{1}H$, along with ^{12}C, ^{19}F, ^{31}P, ^{35}Cl and ^{30}Si. The NanoSIMS was used in multicollection mode with each species assigned a detector. The beam current was 10nA, the primary accelerating voltage of the Cs^+ beam was 8kV and the sample was held at -8kV, leading to an impact energy of 16 keV. A 20 x 20 μm raster was pre-sputtered for two minutes to remove surface contamination, followed by a 10 x10 μm^2 raster sputtered for seven minutes for data collection. Using electronic gating, secondary ions from only the central 85% of the raster were collected, which occurred in five blocks of 10

integrations, generating average ion intensities (counts/s) and an estimate of precision (standard errors). All secondary-ion counts measured were normalized to ^{30}Si to adjust for fluctuations in the primary ion beam current.

In accordance with recommendations by Koga et al. (2003) and Mosenfelder et al. (2011), calibrations were fit with weighted-orthogonal-distance-regressions (W-ODR), which is similar in performance to the common York method (York, 1966, 1969; Wu et al., 2018). This optimization method minimizes the distance between the x and y positions of the calibration line and the data, and also accounts for each data point's uncertainty. We find weighted linear regression an improvement over unweighted regressions because samples often have uncertainties proportional to their concentrations and therefore inclusion of standards with higher concentrations may bias unweighted calibration lines. Prediction interval uncertainties were determined from the central 95% of a histogram composed of 5000 bootstrapped analyses and recalculated W-ODR lines. Additionally, as discussed in detail below, we fit a y-intercept to our calibration lines, which provides an assessment of the true blank (i.e., the $^{16}OH/^{30}Si$ signal at zero ppm H_2O). As explained below, to further improve calibrations at low concentrations our final calibration lines were fit including a near-blank standard (either SynFo100 or Suprasil glass). This step better accounts for uncertainty in the calibration line at low concentrations. Prior to fitting calibrations, $^{16}OH/^{30}Si$ measurements were multiplied by the known SiO_2 wt% concentration of each standard to correct for differences in silica between phases.

FINDINGS

4.1.Calibration Evaluation

We first present and evaluate the SIMS measurements of the Withers12 olivine standards and the calibration formed. This is followed by an examination of the Bell03 calibration for H_2O in

olivine, which is based on a number of natural olivines (Table 1) but ultimately relies on the Bell03 olivine standards.

Withers et al. (2012) SIMS Olivine Calibration

The olivine standards of Withers12 are shown in Figure 1a,b, where SiO_2-corrected $^{16}O^1H/^{30}Si$ ion ratios are plotted against published H_2O concentrations. To first order, the Withers olivine measurements form a tightly constrained calibration line with minimal spread of the error envelope on the regression (e.g., ~5 % at 1000 ppm; Fig. 1b). In detail, however, this high precision only holds well for the elevated H_2O concentrations characteristic of the Withers samples (283 – 2016 ppm). At lower concentrations (Fig. 1a), those most relevant to natural olivines, the calibration is imprecise with a large error envelope on the regression (e.g., ~75 to 150 ppm at ~0.5 OH/Si*SiO_2).

Aside from greater uncertainty at low concentrations, the Withers olivine calibration line also has a y-intercept of 64 +/- 24.5 ppm. In the format plotted in Figure 1, a calibration line should produce a slightly negative y-intercept, which translates to a positive x-intercept, indicative of the signal produced at a true blank of zero ppm H (i.e., some hydrogen will always be detected despite the rigorous steps taken to minimize contamination). The orthopyroxene standards and calibration line are also shown in Figure 1 to demonstrate a calibration that meets this criterion; the near-blank standard (Suprasil 3002 SiO_2 glass with approximately 1 ppm H_2O certified by its manufacturer Heraeus Conamic; Kumamoto et al., 2017; Heraeus, 2019; Heraeus, 2020) plots directly on the independently-determined orthopyroxene calibration line (which does not include Suprasil in its regression). We interpret the high y-intercept of the calibration line for the Withers12 olivine standards as systematic error in their published ERDA values. This

interpretation is supported by the blank Withers12 measured during their ERDA session of 54 +/- 10 ppm. Withers12 chose not to subtract the ERDA blank because it was trivial compared to their high sample concentrations. Because we have measured a similar y-intercept in the SIMS data, we conclude that the ERDA olivine blank is meaningful, and should be subtracted from the published concentrations in order to most accurately characterize olivines with H_2O concentrations lower than the olivine calibration standards by SIMS. Subtracting the ERDA blank from the SIMS measurements does not change the Withers12 FTIR calibration.

At low H_2O concentrations characteristic of natural olivines we also need to account for SIMS blanks (the instrument's background $^{16}OH/^{30}Si$ signal). The concurrent measurement during calibration of nearly dry samples (near-blanks) provides an important check on calibration accuracy at low concentrations. Ideally the blank would be the same phase as the calibration standards, but often this is not feasible. Commonly used blanks for measuring H_2O in NAMS include the Suprasil glass noted above or a synthetic forsterite sample known as SynFo100 (Koga et al., 2003). Either should be an appropriate blank for NAMs calibrations because $^{16}OH/^{30}Si$ ratios are multiplied by SiO_2 and the uncertainty on the known H_2O concentrations is larger than potential mismatched-matrix effects. In addition to providing a check on calibration accuracy at low concentrations, we further improve our calibrations at lower concentrations (< ~20 ppm) by including these near-blank samples in the regression. All other calibration lines presented here are fit through blanks of either SynFo100 or Suprasil glass, depending on which was measured during analysis.

Our preferred calibration line for the Withers12 olivines is shown in Figure 2, with the concentrations corrected for the ERDA blank of 54 +/- 10 ppm and the calibration line fit through Suprasil. Note the relative improvement of the error envelope on the regression at low

concentrations as a result of including Suprasil in the calibration line. These samples form a calibration slope with an improved y-intercept value of -3.4 +/- 0.3 ppm, compared to the uncorrected SIMS calibration intercept of 64 +/- 24.5 ppm noted above.

Bell et al. (2003) SIMS Olivine SIMS Calibration.

All of the Bell03 olivine standards have lower reported H_2O concentrations (≤ 245 ppm) than the Withers12 standards (≥ 283 ppm; Table 1). In order to compare the two sets of samples, we expanded the scale in Figure 2a to examine lower H_2O concentrations, which reveals a number of problems in the Bell calibration. The most obvious is that the six repeat SIMS measurements of standard KLV-23 vary by a factor of ~3. Mosenfelder et al. (2011) observed this same variation using different instruments (The Cameca 7fGeo and NanoSIMS 50L at Caltech's Center for Microanalysis) and attributed it to heterogeneous hydrous brucite inclusions, which are resolvable by SIMS but not by the NRA measurements in Bell03. The other Bell03 standard measured here, GRR1012, also contains hydrous inclusions (Mosenfelder et al., 2011) and also shows variability in many SIMS calibrations (Supplemental Fig. S1). Nano-SIMS measurements containing these hydrous non-olivine phases can often be identified by comparing the expected Poisson error of the ion-counting statistics ($\sigma_{Poisson}$) with the standard error on the mean of the five integrated counting blocks(σ_{mean}) (Fitzsimons et al. 2000). Mosenfelder et al. (2011) recommend discarding measurements with a $\frac{\sigma_{mean}}{\sigma_{Poisson}} > 5$. While this criterion is useful it does not always improve the precision of the calibration. Supplemental Fig. S2 demonstrates with the standard KLV-23 that filtering data points for homogeneity actually reduced the precision of the mean. Thus, these standards are problematic from both the

perspective of sample heterogeneity at multiple scales, and from hydrous non-olivine phases contributing to the NRA determinations of H_2O concentration.

These issues lead to the relatively low R^2 value of 0.77 and an uncertainty of the error envelope on the regression of ~20% at 200 ppm for the Bell03 standards in Fig. 2 for the June 2017 session. The August 2016 calibration line based on Bell03 olivines (Supplementary Figure S1) is seemingly more precise with a R^2 of 0.93 but still suffers from many of the sample problems as noted above. Not only is it apparent that KLV-23 is heterogeneous, but GRR1012 is as well. Some of the improvement in the fit of this line compared to that for the June 2017 data is likely an artifact of the fact that ROM250-13 was not measured during this session, and thus there is apparently less inter-standard variability.

DISCUSSION

Our findings highlight the problems and limitations in current approaches to the quantification of H_2O concentrations in olivine, and suggest a path forward by using an orthopyroxene calibration, as recommended by Kumamoto et al. (2017). Below we explore this approach further, and provide recommendations to achieve more precise measurements of H_2O concentrations in olivine and orthopyroxene by both SIMS and FTIR. In addition, by applying this improved standardization approach to published data, we bring into closer agreement the widely varying estimates of the partition coefficient for H_2O between olivine and melt (at ~0.2 -2 GPa).

Mismatch Between the Bell and Withers Olivine Standard Calibrations.

In addition to the problems with the olivine standard calibrations discussed above – heterogeneity in the natural Bell03 olivines and high blank for the synthetic Withers12 olivine ERDA data – the two calibration curves have dramatically different slopes, with the Bell03 slope

greater by a factor of about two (Fig 2). Withers12 noted a similar difference in their FTIR calibration compared to that of Bell03, resulting in H_2O concentrations that differ by -37% ($\frac{Withers12}{Bell03} - 1$) ±5% (1 sigma) for the same samples.

The source of the offset between Bell03 and Withers12's infrared-molar absorptivity is not readily apparent from examining FTIR spectra in the OH-stretching region (3000 – 3750 cm^{-1}) for the olivines from each study (Fig S3). A wavenumber dependent molar absorptivity, such as that used by Libowitsky and Rossman (1997), cannot resolve the disagreement because both sets of spectra are dominated by bands in the same range between 3500 and 3550 cm^{-1}. In fact, the weighted-average wavenumber (as defined by Libowitsky and Rossman (1997)) for the Withers12 spectra ranges from 3417 to 3547 cm^{-1} and all of the ERDA and FTIR measurements are well fit using a single molar absorptivity. The range in average wavenumber is applicable to many natural olivines, including those of Bell03. This assessment is supported by Mosenfelder et al. (2011) who also do not find any evidence for a wavenumber dependent molar absorptivity in olivines dominated by OH-stretching bands above 3450 cm^{-1}.

The SIMS measurements we report for these samples demonstrate that the Bell03 and Withers12 olivines fall on different slopes (Fig. 2) due to differences in the NRA and ERDA measurements, independent of any differences in their IR absorption characteristics. The -51±7% ($\frac{Withers12}{Bell03} - 1$) difference in the Withers12 and Bell03 calibration slopes determined by SIMS is within 2σ of the -37±5% difference in FTIR molar absorptivities. SIMS is not as, if at all, sensitive to the bonding environment of H in olivine compared to FTIR and thus differences in trace element content should have little effect on SIMS measurements of $^{16}O^{1}H$ with a Cs^{+} beam. In fact, Mosenfelder and Rossman (2013) found no meaningful matrix effects related to comparably large differences in iron concentration for orthopyroxene measurements (Mg#: 79 –

99). The difference in the IR absorption coefficients determined by Bell03 and Withers12 is entirely consistent with the differences between the NRA and ERDA measurements as revealed in our SIMS measurements, and may not be strongly affected by the different hydrous defects evidenced in the IR measurements.

Knowing that the NRA measurements of KLV-23 and GRR1012 also included hydrous non-olivine phases, it follows that the derived concentrations of H_2O in olivine for both samples are overestimates. The nano-SIMS measurements of KLV-23 provide some insights as to the heterogeneity of H_2O in the sample in the area of each raster (10μm x 10μm). The nano-SIMS measurements of KLV-23 from August 2016 and June 2017 average ~140 ppm H_2O, the concentration measured by NRA, regardless of the degree of heterogeneity as reflected in $\frac{\sigma_{mean}}{\sigma_{Poisson}}$ (Fig. S2). In the case of the three most homogenous ($\frac{\sigma_{mean}}{\sigma_{Poisson}} < 2$) nano-SIMS measurements on KLV-23 the two data points with the lowest concentrations (85 and 95 ppm) are (38% and 30%) lower than the mean value. Thus the nano-SIMS data demonstrate both the presence of hydrous domains in KLV-23 and a lower concentration in the olivine than determined by bulk NRA measurements. It is also unlikely that hydrous non-olivine inclusions generate a proportionally equal contribution to the total IR absorbance and the NRA measurements. The effect of heterogeneities in the IR path on the FTIR spectrum can be complex and difficult to model with the Beer-Lambert law (Mayerhöfer et al., 2016, 2020). However, if we assume that the majority of the hydrous inclusions absorb IR at wavenumbers distinct from hydrous olivine defects (3000-3650 cm^{-1}), we can revise the integrated absorbance of the Bell03 olivines to exclude those other wavenumbers (>3650 cm^{-1}) and compare directly to the SIMS measurements and the Withers12 olivines. Such a comparison (Fig. 3) reveals a closer agreement between Bell03 and Withers12 olivines than in Fig. 2. This suggests that the offset in the Bell03

and Withers12 olivines is in the NRA-ERDA data more than any large difference in the IR absorbance behavior. A more detailed reassessment of the IR vs. SIMS data is difficult, however, due to the heterogeneities in the Bell03 samples, which ultimately limits their use as reference materials.

The Withers12 ERDA measurements, on the other hand, are comparably more robust. After mapping H_2O concentrations across the samples, Withers et al. found them to be largely homogenous and carefully excluded regions of anomalously high concentration due to surface contamination from the ERDA analyses. While the ERDA blank (54 +/- 10 ppm) is higher than the Bell03 NRA blank (2 +/- 2ppm), the Withers samples are higher in H_2O concentration and thus the blank is easily corrected for and has little effect on the FTIR or SIMS calibrations.

An Alternative Olivine Calibration using Orthopyroxene

Given the inherent difficulty of overcoming the problem of heterogeneity for the Bell03 natural olivine standards, and the fact that the Withers12 synthetic standards are not widely available, we explore the use of orthopyroxene as an alternate calibration standard, as previously suggested by Kumamoto et al. (2017).

Previous authors have suggested that SIMS calibration lines for H_2O in mafic natural olivines and orthopyroxenes should have similar slopes due to their similar major element compositions (Koga et al., 2003; Mosenfelder and Rossman, 2013a; Kumamoto et al., 2017). The natural orthopyroxene standards in common use (Table 1) are more homogeneous for H_2O concentration than the Bell03 natural olivine standards. Indeed, the replicate measurements of the three orthopyroxene standards consistently measured at Carnegie show little variation; the

range in each standard's measured replicate $^{16}O^{1}H/^{30}Si$ ratios (India Enstatite: 15.0%; KBH-1: 2.3%; ROM273: 0.65%) is considerably smaller than the >40% found in the two Bell03 olivine standards (KLV-23: Fig 2a, Fig. S1. S2; GRR1012 Fig. S1). Furthermore, the orthopyroxene standards form a more robust calibration line than the Bell03 olivine standards ($R^2 = 0.995$), with a 95% confidence interval of <±5% (Fig. 1, Table 1). The precision of the orthopyroxene Nano-SIMS calibration line supports the use of the Bell et al. (1995) orthopyroxene FTIR calibration, as concluded by Mosenfelder and Rossman (2013). Below we discuss the merits of, and suggest modifications to, the use of the orthopyroxene calibration line for the calibration of olivine.

The community has begun to use a new set of orthopyroxene standards published by Kumamoto et al. (2017) and archived at the Smithsonian Institution. Ten of the 15 Kumamoto et al. (2017) orthopyroxene standards were measured in the August 2016 and June 2017 sessions (Table 2 and 3 and Fig. 4). These measurements provide an independent opportunity to compare the Kumamoto standard values to the Carnegie orthopyroxene calibration. Differences are expected to be small because the Kumamoto values were obtained at Carnegie using the same three Carnegie orthopyroxene standards (India Enstatite, KBH-1, and ROM273). The results from the two Carnegie Nano-SIMS sessions are within 10% of the published Kumamoto et al. (2017) values. For two Kumamoto et al. (2017) standards, however, SIMS measurements vary significantly, possibly due to heterogeneity within these particular standards (SMNH ID:109426-1 and 117322-245).

In order to demonstrate that the SIMS orthopyroxene and olivine calibrations are stable relative to each other, we examined the data from 12 Carnegie SIMS sessions from 2007 to 2019. We treated the olivine standards as unknowns and calculated H_2O concentrations for each SIMS measurement with the orthopyroxene calibration for that SIMS session (Fig. S4). For the most

consistent olivine samples (e.g. CM58-ol, ROM250-13), the standard deviation (1 sigma) of the concentrations is 12-14%. This uncertainty is comparable to the concentration variations measured in a single sample during the same session supporting the reproducibility and stability of olivines measurements relative to the orthopyroxene calibration with time.

As was shown in Figure 2, the orthopyroxene calibration line lies between the olivine calibration lines for the standards of Bell03 and Withers12. However, the slope of the orthopyroxene calibration line is closer to that for the Withers olivines, differing only by 19% (Fig. 2a). The first-order similarity in the slopes of the orthopyroxene and Withers olivine calibrations lines provides some justification for using the orthopyroxene calibration in future studies. It is possible that the 19% offset is real, resulting from differing matrix effects in the SIMS measurements of olivine and orthopyroxene. But there are also reasons to suspect that the orthopyroxene calibration line is erroneously high, and should be adjusted to a lower slope (Fig. 2a). This is because the orthopyroxene calibration is ultimately based on measurement of a single opx (KBH-1) by manometry (Bell et al., 1995), upon which both the FTIR and SIMS determination of the other orthopyroxene standards are based. That is, the values for the other Carnegie orthopyroxene standards (India Enstatite, and ROM 273) were calibrated based on KBH-1 as an FTIR and/or SIMS reference standard (Koga et al., 2003; Bell et al. 2004, Aubaud et al., 2007). Thus, the validity of the orthopyroxene calibration line depends on the accuracy of the accepted value for H_2O in KBH-1. Bell et al. (1995) recommended a H_2O concentration for KBH-1 of 217 +/- 11 ppm, although they measured 186 +/- 1.6 ppm by manometry. Manometry is a bulk measurement of H_2O extracted by the heating of several grains at once. The rationale for upward adjustment of KBH-1's H_2O concentration rested on a determination that 14% of the H_2O had not been extracted and measured, a finding based on FTIR analyses of a single grain

454 before and after heating. Bell et al. (1995) noted that this upward correction was likely a
455 maximum estimate because the grain measured was one of the largest in their population. The
456 smaller grains in the bulk manometry measurement would have more efficiently released their
457 H_2O (if the process was governed by length-scale dependent diffusion) and therefore would not
458 require the 14% upward correction. For example, a grain with a minimum width 20% smaller
459 would have retained only 4% vs the 14% estimated by Bell et al. (1995) (Fig. S7). We do not
460 know the grain size distribution relative to the single grain measured by Bell et al. (1995) but
461 because the grain was reported as distinctively larger than the others, it is likely that the bulk
462 sample was over-corrected upward. We propose that the standard reference concentration for
463 KBH-1 should be revised to better represent the full range of uncertainty in the published
464 concentrations, recommending the average of the uncorrected (186 ppm; the lowest estimate)
465 and over-corrected (217 ppm; the highest estimate) KBH-1 concentrations, yielding a
466 concentration of 202 ppm ± 15 ppm.

467 Our recommendation of a lower concentration for KBH-1 is counter to the choices made
468 by Mosenfelder et al. (2013a) who supported the use of the Bell et al. (1995) concentration of
469 217± 11, in part based on hydrogen depth profiles of KBH-1 (223 ppm) by proton-proton
470 scattering reported by Wegdén et al. (2005). The latter measurement, however, can support a
471 value anywhere from 181±39 to 219±60 ppm (see table S6 for details). Another independent
472 measurement of KBH-1 using continuous flow mass spectrometry reported a value of 165+/- 20
473 ppm (O'Leary et al., 2007). Unlike Bell et al. (1995), the latter investigators did not directly
474 measure how much H_2O was left unextracted after heating for any of their orthopyroxene grains.
475 While their measurements were shorter than those of Bell et al. (1995) (30 - 90 minutes vs 6
476 hours, respectively), their extractions temperatures were higher (1120 ˚C vs ~1000 ˚C) and their

grains were thinner (<~87μm vs 0.1 to 2mm). Given these uncertainties, we choose not to integrate the Wegdén et al. (2005) and O'Leary et al. (2007) measurements into our recommended value for KBH-1.

Our proposed modification to the concentration of KBH-1 of 202 +/- 15 ppm H_2O would lead to a revised integral molar absorption coefficient of 86600 +/- 7000 $L*mol^{-1} * cm^{-2}$ (the original constant reported in Bell et al. (1995) was 80600 +/- 3200 $L*mol^{-1} * cm^{-2}$). The integral specific absorption coefficient for high-magnesium orthopyroxene is 15.95 +/- 1.23 ppm^{-1} cm^{-2} (originally reported as 14.84 +/- 0.59 ppm^{-1} cm^{-2}). Applying this new coefficient to the other orthopyroxene standards determined by FTIR yields revised values for India enstatite and ROM 273 reported in Table 1.

The revised orthopyroxene standard concentrations proposed here yield a SIMS calibration line that is 12% higher than the Withers12 olivine line, as opposed to the original 19% difference. It is possible the 12% difference is due to real SIMS matrix effects between olivine and orthopyroxene. However, we consider 12% to be within the aggregated uncertainty of the orthopyroxene standard concentrations (resting on KBH-1), and the large blank corrections required for Withers12 olivines (Fig. 1a). We therefore support the recommendation of Kumamoto et al. (2017) to use an orthopyroxene calibration for the SIMS standardization of natural olivines, but using our revised concentrations (Table 1 and the dashed line in Figure 2a). In view of the fact that the Kumamoto orthopyroxene standards are likely to become more widely used for calibrations of both olivine and orthopyroxene, we have suggested new standard H_2O concentrations based on our correction to the KBH-1 and the DTM orthopyroxene standard values. These updated H_2O concentrations are presented in Table 3. We have not proposed adjusted reference concentrations for sample SMNH ID:109426-1 because our measurements

disagree with the results of Kumamoto by more than -10% and the June 2017 measurements vary by ~±20%. Sample SMNH ID:117322-245 is highly variable (±46%) in the June 2017 NanoSIMS measurements therefore we have not considered measurements from this date in the revised reference concentration.

Clinopyroxene Calibrations and Standards

While not the primary subject of this paper, the clinopyroxene standards from Bell et al. (1995) and Bell et al. (2004) were also analyzed in multiple sessions on the Cameca 6F at Carnegie from 2007 - 2019 (and produced data reported in multiple publications, such as Wade et al., 2008; Lloyd et al., 2016 and Kumamoto et al., 2017). The calibrations included the same four standards: PMR-53 (measured by manometry) and ROM271-10, -16 and -21 (measured by FTIR by Bell et al. 2004 and using the molar absorptivity from Bell et al. 1995, which is based on the PMR-53 manometry). The linear fits to these standards have led to high uncertainty in H_2O concentrations, >± 50 ppm for samples with > 200 ppm (Figure S5a). Mosenfelder and Rossman (2013b) determined that the wavenumber-dependent FTIR molar absorptivity of Libowitsky and Rossman (1997) improves the agreement between SIMS and FTIR data. Weiss et al., (2018) make similar but less definite conclusions from their measurement of H_2O in clinopyroxene by proton-proton scattering. Aubaud et al. (2009)'s ERDA measurements of clinopyroxene (including PMR-53 and ROM271 -16, and ROM271-21) also provide some support for using the Libowitsky and Rossman (1997) wavenumber dependent molar absorptivity, but the uncertainty of their blank (102 ±81 ppm) makes it difficult to more precisely determine the concentration of their samples. Our analysis of the Carnegie data further supports this conclusion, reducing the uncertainty on the calibration to ~10% (Fig. S5a). Moreover, we

find that this clinopyroxene calibration line is in close agreement with the basaltic glass calibration line determined by both the NanoSIMS and 6F (Fig. S6). This general agreement in SIMS H_2O calibrations using three independent approaches (Bell et al., (1995)'s manometry measurement of PMR-53, Libowitsky and Rossman's (1997) FTIR absorption coefficients applied to clinopyroxenes, and the basaltic glass SIMS calibration) supports their use and motivates a re-examination of the Kumamoto et al. (2017) clinopyroxenes. The published concentrations for these openly-accessible standards were determined using the lower quality Bell et al. (1995) calibration (e.g., the red line in Fig S5a). Eleven of the twelve Kumamoto clinopyroxenes were analyzed in the August 2016 and June 2017 NanoSIMS sessions at Carnegie, and we illustrate the excellent agreement in values (within 10%, Fig S5b) calibrated using basaltic glasses and with the clinopyroxene calibration (with reference concentrations determined using the wavenumber-dependent FTIR molar absorptivity of Libowitsky and Rossman (1997)). Revised values for the Kumamoto clinopyroxenes based on the average of the two calibration approaches shown in Fig S5b are provided in Table 3. Revised values for clinopyroxenes from Bell et al. (2004; ROM271-10, -16 and -21) are provided in supplemental table S5.

Application to an improved partition coefficient for H_2O between olivine and melt

An important application that follows from more accurate measurements of H_2O concentrations in olivine is the partitioning of H_2O between olivine and melt. There is currently significant disagreement in the partition coefficients (K_d) determined from experimental studies at upper mantle pressures (~0.2 - 2 GPa) (Koga et al. 2003; Aubaud et al., 2004; Hauri et al., 2006; Tenner et al., 2009) and those measured in magmatic olivine in hydrous arc basalts and

their entrapped melt-inclusions (Le Voyer et al. 2014; Newcombe et al., 2020). Experimentally determined olivine-melt partition coefficients for H_2O are nearly double those based on natural samples (Fig. 5a).

The main source of this disagreement has been attributed to diffusive H^+ loss from the olivine phenocrysts surrounding melt inclusions (Le Voyer et al. 2014, Newcombe et al. 2020, Barth and Plank, 2021). In this scenario, olivine loses H^+ through magmatic degassing upon ascent, and therefore the apparent K_d will be lowered as a function of the extent of H^+ loss. Because diffusive H^+ loss varies by several orders of magnitude along the different crystallographic axes (Demouchy and Mackwell, 2006), the apparent K_d will also depend on the position of the SIMS analysis with regard to the olivine crystallographic axes and its distance from the interface between the melt inclusion and that olivine (Le Voyer et al., 2014). These factors will all tend to skew the apparent K_d for studies of melt inclusions to lower values than experimental studies.

While H^+ loss is a reasonable explanation for the lower K_d in natural samples, a major source of the discrepancy lies in the different olivine calibrations used by the different studies. We can explore this because several SIMS studies used both olivine and orthopyroxene calibration lines (Koga et al., 2003; Aubaud et al., 2004; Hauri et al., 2006; Newcombe et al., 2020). Using the orthopyroxene calibrations as recommended above, we have recalculated the K_d values for olivine-melt pairs in both the experimental and melt inclusion studies. As shown in Figure 5b the recalibration of the K_d data now brings the experimental and melt inclusion datasets into closer agreement. The K_d values of Koga et al. (2003), Aubaud et al. (2004) and Hauri et al. (2006) are reduced by factors of ~35-40% using our recommended calibration and are also consistent with the 37 +/- 5% reduction in using Withers vs. Bell FTIR absorption coefficients. The notable

570 exceptions are the three olivine-melt inclusion measurements of Newcombe et al. (2020) which
571 are only reduced by 7%; this is because they followed the recommendation of Kumamoto et al.
572 (2017) and mainly used the Carnegie orthopyroxene standards for their SIMS olivine analyses.
573 We have only revised the Newcombe et al. (2020) results slightly to account for our proposed
574 revisions to the orthopyroxene standard H_2O concentrations. Taken together, the experimental
575 and natural datasets are consistent with an average K_d of 0.0009 +/- 0.0003.

576 For the average K_d above, we do not include the data of Portnyagin et al. (2008) who
577 reported K_d of 0.0022–0.0027 for experimentally equilibrated olivines hosted melt inclusions.
578 These measurements are seemingly ideal to resolving the question of differences between melt
579 inclusion studies and other experimental studies, but we have cause to think their measurements
580 of H_2O in olivine are skewed to higher concentrations. Unlike the other analyses included in
581 Figure 5, which were made by SIMS, Portnyagin et al. (2008) measured H_2O concentrations in
582 olivine by FTIR. They followed the method of Matveev and Satchel (2007), which is a hybrid of
583 the Bell03 calibration and the wavenumber-dependent calibrations of Libowitsky and Rossman
584 (1997). The analyses used an unpolarized IR-beam measured nearly perpendicular to the
585 crystallographic directions that have the strongest absorbance signal, [100] and [001] and thus
586 likely represent a maximum of the combined signal for all three axes. Even so, we can still
587 estimate that the Withers12 equivalent K_d values for these samples would be 0.0013–0.0016,
588 only slightly higher than the highest estimates by SIMS.

589 Le Voyer et al. (2014) also measured partition coefficients in melt inclusions and olivine
590 host pairs. They observed steep gradients in olivine H_2O concentration surrounding melt
591 inclusions which were consistent with diffusive H^+ loss during magmatic ascent and represent a
592 challenge to the olivine measurements. They report partition coefficients of 0.0007 – 0.0003

593 based on the olivine measurement taken closest to the melt inclusion. Le Voyer et al. (2014) do
594 not report an orthopyroxene SIMS calibration, so unlike the other studies we have no direct
595 comparison with the results of our study. They do, however, measure the homogenous olivine
596 standards recommended by Mosenfelder et al. (2011) which are consistent with the Bell03 FTIR
597 calibration. If we apply a conversion factor of 0.63 +/- 0.08 to translate data reported using the
598 Bell absorption coefficient to that of Withers, the rescaled partition coefficients from Le Voyer et
599 al. (2014) are lower on average than those of Newcombe et al. (2020) and most of the
600 experimentally determined values. We cannot rule out that H_2O partition coefficients determined
601 from melt inclusion studies are systematically too low, in view of the observed diffusive H^+ loss
602 gradients described above.

603 The heart of the issue is whether K_d values from equilibrium experiments can be applied
604 to magmatic olivines often formed at lower pressures than the experimental samples (Newcombe
605 et al., 2020). Our results support the use of the experimental K_d. Much of the offset between
606 analyses of natural olivine-melt inclusion pairs and experimental K_d values is resolved by our
607 proposed recalibration of the SIMS data. As noted above, we believe the remaining offset is
608 caused by H_2O loss from natural olivine phenocrysts during magma ascent. If K_d and pressure do
609 in fact correlate at less than 2 GPa, as is seen at greater pressures (Adam et al., 2016), it cannot
610 be resolved with the current datasets. Further experimental studies at lower pressures relevant to
611 magmatic ascent would be useful in resolving remaining questions.

612 ## IMPLICATIONS

613 The measurement of H_2O concentrations in olivine has presented a great analytical challenge.
614 The literature is rife with inconsistencies that have derived from evolving FTIR techniques,
615 heterogeneous standard reference materials, and signals near detection limits. Most data prior to

616 the mid-1990's relied on Paterson's foundational work determining FTIR based calibrations for
617 H_2O in glasses and quartz. Bell et al. (1995) demonstrated in their landmark study that Paterson's
618 (1982) calibration could result in H_2O concentrations up to 3x too low compared to mineral
619 specific calibrations for NAMS, with dramatically different implications for the effect of
620 hydration on seismic attenuation, mantle viscosity and solidus. The development by Bell et al.
621 (2003) and Withers et al. (2012) of independent datasets for H_2O concentrations in olivine using
622 NRA and ERDA, respectively, was a major step forward, but ultimately led to a ~40%
623 uncertainty in the FTIR absorption coefficients in use over the past ten years.

624 Our work has clearly shown that the ~40% offset between Bell03 and Withers12 absorption
625 coefficients lies largely within the NRA vs ERDA analyses, more than any major difference in
626 the IR absorption characteristics of the two sets of olivines. The NRA H_2O concentrations
627 measured by Bell03 are likely contaminated by the presence of hydrous inclusions (well
628 documented by Mosenfelder et al., 2011). Taken together, our results do not support the use of
629 the Bell03 FTIR absorption coefficient for quantifying H_2O in olivine.

630 Our work highlights a general problem in developing SIMS calibration lines using natural
631 olivines: many with high concentrations of H_2O (e.g., > 100 ppm, which is desirable for a
632 calibration) contain hydrous inclusions. This has plagued the use of the natural olivine
633 standards. Alteration/weathering of olivine remains an important issue when considering the
634 reliability of H_2O measurements in standards or samples, especially extraterrestrial ones
635 (Hausrath et al., 2008; Stephant et al., 2018). On the other hand, natural orthopyroxenes have
636 both higher typical concentrations and are less affected by hydrous inclusions than natural
637 olivines. Our study has attempted to reconcile these inconsistencies in the olivine standards (to

638 within 12%, largely within analytical precision) and points to a path forward using
639 orthopyroxenes, with the following recommendations and implications.

640 • The values of the synthetic olivine standards developed by Withers et al. (2012) require
641 correction for the 54 +/- 10 ppm ERDA blank measured in that study (Table 1). This
642 becomes important when applying this calibration to natural olivine samples, which
643 typically have lower concentrations.

644 • Examination of the Bell et al. (2003) calibration using natural olivine standards confirms
645 the findings of Mosenfelder et al. (2011) that two of the three standards are
646 heterogeneous with respect to H_2O and therefore problematic to use as standards.
647 Moreover, the presence of hydrous inclusions in these standards means that the bulk
648 NRA analyses in Bell et al. (2003) are skewed to higher concentrations than in the
649 inclusion-free olivine, rendering these olivine grains unreliable as standards.

650 • The difficulties of using olivine calibration standards can be avoided by using
651 orthopyroxenes as standards for the calibration of H_2O in olivine by SIMS, as previously
652 suggested by Kumamoto et al. (2017). Our analysis shows that the Carnegie SIMS
653 calibration of olivines using orthopyroxene standards is highly stable over time (within
654 11-14% relative).

655 • The SIMS olivine calibration line based on Withers's olivines, however, is offset by 19%
656 from the calibration line for orthopyroxene. To explore this discrepancy, we traced the
657 basis for the accepted values for the orthopyroxene standards to the one underlying
658 measurement – the manometry value of KBH-1 reported by Bell et al. (1995). Our
659 interpretation of their data suggests a modification of the reference value from 217+/-11

This is the peer-reviewed, final accepted version for American Mineralogist, published by the Mineralogical Society of America.
The published version is subject to change. Cite as Authors (Year) Title. American Mineralogist, in press.
DOI: https://doi.org/10.2138/am-2022-8247. http://www.minsocam.org/

660 ppm to 202+/-15 ppm. This leads to modified reference values for all of the
661 orthopyroxene standards measured (Table 1) and a closer approach to the Withers'
662 olivine calibration (within 12%).

663 • Using the new orthopyroxene-based calibration to recalculate previously measured H_2O
664 concentrations in natural and experimental olivines, we determine revised values for the
665 partition coefficient for H_2O between olivine and melt of 0.0009 +/- 0.0003 at pressures
666 between ~0.2 and 2 GPa. This also appears to resolve much of the previous discrepancy
667 in the partition coefficients between experimental studies and those based on natural
668 olivine-hosted melt inclusion samples.

669

670 The following summarizes our proposed best practices when measuring H_2O concentrations in
671 olivine by SIMS:

672 • At the present time, SIMS measurements of H_2O in olivine should be calibrated to well-
673 characterized orthopyroxene standards, which we find to be most consistent with the
674 Withers et al. (2012) olivine calibration. Currently these include orthopyroxenes of Bell
675 et al. (1995), Mosenfelder et al. (2013a), and Kumamoto et al. (2017), with adjustments
676 to reference values as noted in Table 3. In cross-mineral calibrations it is important to
677 multiply SIMS $^{16}O^{1}H/^{30}Si$ ratios by the SiO_2 wt.% concentration of each sample.
678 • Calibration lines should use weighted-linear regression. In order to test for goodness of
679 fit, regression through the standards (not including the blank) should determine the Y-
680 intercept, which should then be compared with a "blank" measurement. Assuming the
681 initial Y-intercept agrees with the blank within error, the final calibration line should be

re-fit to include the blank in the regression. This better accounts for uncertainty in the blank measurement at low concentrations.

- Finally, we suggest that future work be done to further refine the calibrations for olivine and orthopyroxene. The same set of homogenous samples, natural and synthetic, should be measured by multiple methods (ERDA, NRA, Manometry, SIMS and FTIR) to determine the most accurate and precise calibration. In the interim, homogenous olivine standards (e.g., CM58-ol) should continue to be measured and reported. This will help ensure that future calibrations can be updated if the olivine calibration is revised with additional data. New homogenous olivines standards should be developed and made available, as has been done for pyroxenes by Kumamoto et al. (2017).

ACKNOWLEDGEMENTS

We are indebted to Anthony Withers who provided to EHH his synthetic olivines. We thank Elizabeth Ferriss and Samer Naif for their work developing and organizing the 2016 workshop on the Electrical Conductivity of olivine hosted at the Carnegie Institution of Washington with support from the Cooperative Institute for Dynamic Earth Research. That workshop led to the acquisition of the SIMS calibrations studied here. We are grateful for the help and ingenuity of Jianhua Wang while collecting SIMS data at Carnegie over the course of many analytical sessions. We would like to thank Anna Barth and Megan Newcombe for their insights into this subject matter. We are grateful to Rick Hervig, Peter Tollan and Jed Mosenfelder for their thorough reviews, and Anne Peslier for her keen insights and essential guidance as Editor. This work was supported by the National Science Foundation under grant no. EAR-1731784 to T.P. and grant no. DGE 2036197 to W.H.T. under the NSF's Graduate Research Fellowship Program.

705 **References**

706

707 Adam, J., Turner, M., Hauri, E.H., and Turner, S. (2016) Crystal/melt partitioning of water and
708 other volatiles during the near-solidus melting of mantle peridotite: Comparisons with non-
709 volatile incompatible elements and implications for the generation of intraplate magmatism.
710 Science (New York, N.Y.), 101, 876–888.
711 Asimow, P.D., Stein, L.C., Mosenfelder, J.L., and Rossman, G.R. (2006) Quantitative polarized
712 infrared analysis of trace OH in populations of randomly oriented mineral grains. American
713 Mineralogist, 91, 278–284.
714 Aubaud, C., Hauri, E.H., and Hirschmann, M.M. (2004) Hydrogen partition coefficients between
715 nominally anhydrous minerals and basaltic melts. Geophysical Research Letters, 31, 2–5.
716 Aubaud, C., Withers, A.C., Hirschmann, M.M., Guan, Y., Leshin, L.A., Mackwell, S.J., and
717 Bell, D.R. (2007) Intercalibration of FTIR and SIMS for hydrogen measurements in glasses
718 and nominally anhydrous minerals. American Mineralogist, 92, 811–828.
719 Aubaud, C., Bureau, H., Raepsaet, C., Khodja, H., Withers, A.C., Hirschmann, M.M., and Bell,
720 D.R. (2009) Calibration of the infrared molar absorption coefficients for H in olivine,
721 clinopyroxene and rhyolitic glass by elastic recoil detection analysis. Chemical Geology,
722 262, 78–86.

723

724 Balan, E., Ingrin, J., Delattre, S., Kovács, I., and Blanchard, M. (2011) Theoretical infrared
725 spectrum of OH-defects in forsterite. European Journal of Mineralogy, 23, 285–292.
726 Barth, A., and Plank, T. (2021) The Ins and Outs of Water in Olivine-Hosted Melt Inclusions:
727 Hygrometer vs. Speedometer. Frontiers in Earth Science, 9, 1–17.

728 Beer (1852) Bestimmung der Absorption des rothen Lichts in farbigen Flüssigkeiten. Annalen
729 der Physik, 162, 78–88.
730 Bell, D.R., Ihinger, P.D., and Rossman, G.R. (1995) Quantitative analysis of trace OH in garnet
731 and pyroxenes. American Mineralogist, 80, 465–474.
732 Bell, D.R., Rossman, G.R., Maldener, J., Endisch, D., and Rauch, F. (2003) Hydroxide in
733 olivine: A quantitative determination of the absolute amount and calibration of the IR
734 spectrum. Journal of Geophysical Research: Solid Earth, 108, 1–9.
735 Bell, D.R., Rossman, G.R., and Moore, R.O. (2004) Abundance and partitioning of OH in a
736 high-pressure magmatic system: Megacrysts from the monastery kimberlite, South Africa.
737 Journal of Petrology, 45, 1539–1564.
738 Berry, A.J., Hermann, J., O'Neill, H.S.C., and Foran, G.J. (2005) Fingerprinting the water site in
739 mantle olivine. Geology, 33, 869–872.
740 Berry, A.J., O'Neill, H.S.C., Hermann, J., and Scott, D.R. (2007) The infrared signature of water
741 associated with trivalent cations in olivine. Earth and Planetary Science Letters, 261, 134–
742 142.
743 Blanchard, M., Ingrin, J., Balan, E., Kovács, I., and Withers, A.C. (2016) Effect of iron and
744 trivalent cations on OH-defects in olivine.
745 Bureau, H., Raepsaet, C., Khodja, H., Carraro, A., and Aubaud, C. (2009) Determination of
746 hydrogen content in geological samples using elastic recoil detection analysis (ERDA).
747 Geochimica et Cosmochimica Acta, 73, 3311–3322.
748 Demouchy, S., and Bolfan-Casanova, N. (2016) Distribution and transport of hydrogen in the
749 lithospheric mantle: A review. Lithos, 240–243, 402–425.
750 Demouchy, S., and Mackwell, S. (2006) Mechanisms of hydrogen incorporation and diffusion in

751 iron-bearing olivine. Physics and Chemistry of Minerals, 33, 347–355.
752 Demouchy, S., Jacobsen, S.D., Gaillard, F., and Stem, C.R. (2006) Rapid magma ascent recorded
753 by water diffusion profiles in mantle olivine. Geology, 34, 429–432.
754 Endisch, D., Sturm, H., and Rauch, F. (1994) Nuclear reaction analysis of hydrogen at levels
755 below 10 at.ppm. Nuclear Inst. and Methods in Physics Research, B, 84, 380–392.
756 Faul, U.H., Cline, C.J., David, E.C., Berry, A.J., and Jackson, I. (2016) Titanium-hydroxyl
757 defect-controlled rheology of the Earth's upper mantle. Earth and Planetary Science Letters,
758 452, 227–237.
759 Ferriss, E., Plank, T., Newcombe, M., Walker, D., and Hauri, E. (2018) Rates of dehydration of
760 olivines from San Carlos and Kilauea Iki. Geochimica et Cosmochimica Acta, 242, 165–
761 190.
762 Fitzsimons, I.C.W., Harte, B., and Clark, R.M. (2000) SIMS stable isotope measurement:
763 counting statistics and analytical precision. Mineralogical Magazine, 64, 59–83.
764 Gaetani, G.A., and Grove, T.L. (1998) The influence of water on melting of mantle peridotite.
765 Contributions to Mineralogy and Petrology, 131, 323–346.
766 Gardés, E., Gaillard, F., and Tarits, P. (2017) Toward a unified hydrous olivine electrical
767 conductivity law Emmanuel. Geochemistry, Geophysics, Geosystems, 1–26.
768 Hauri, E., Wang, J., Dixon, J.E., King, P.L., Mandeville, C., and Newman, S. (2002) SIMS
769 analysis of volatiles in silicate glasses. Chemical Geology, 183, 99–114.
770 Hauri, E.H., Gaetani, G.A., and Green, T.H. (2006) Partitioning of water during melting of the
771 Earth's upper mantle at H2O-undersaturated conditions. Earth and Planetary Science
772 Letters, 248, 715–734.

773 Hausrath, E.M., Navarre-Sitchler, A.K., Sak, P.B., Steefel, C.I. and Brantley, S.L. (2008) Basalt
774 weathering rates on Earth and the duration of liquid water on the plains of Gusev Crater,
775 Mars. Geology 36, 67-70.)
776 Heraeus Quartz North America LLC (2019) Quartz Glass for Optics Data and Properties.
777 Heraeus Brochure. Retrieved from
778 https://web.archive.org/web/20200921193545/https:/www.heraeus.com/media/media/hca/d
779 oc_hca/products_and_solutions_8/optics/Fused_Silica_for_Applications_in_the_NIR_EN.p
780 df
781 Heraeus Quartz North America LLC (2020) Fused Silica for Applications in the Near Infrared (
782 NIR). Heraeus Brochure. Retrieved from
783 https://web.archive.org/web/*/https://www.heraeus.com/media/media/hca/doc_hca/products
784 _and_solutions_8/optics/Fused_Silica_for_Applications_in_the_NIR_EN.pdf
785 Hirschmann, M.M., Ghiorso, M.S., and Stolper, E.M. (1999) Calculation of peridotite partial
786 melting from thermodynamic models of minerals and melts. II. Isobaric variations in melts
787 near the solidus and owing to variable source composition. Journal of Petrology, 40, 297–
788 313.
789 Hirth, G., and Kohlstedt, D.L. (1996) Water in the oceanic upper mantle: implications for
790 rheology, melt extraction and the evolution of the lithosphere. Earth and Planetary Science
791 Letters, 144, 93–108.
792 Jollands, M.C., Kempf, E., Hermann, J., and Müntener, O. (2019) Coupled inter-site reaction and
793 diffusion: Rapid dehydrogenation of silicon vacancies in natural olivine. Geochimica et
794 Cosmochimica Acta, 262, 220–242.
795 Jollands, M.C., St.c. O'Neill, H., Berry, A.J., Le Losq, C., Rivard, C., and Hermann, J. (2021) A

combined Fourier transform infrared and Cr K-edge X-ray absorption near-edge structure spectroscopy study of the substitution and diffusion of H in Cr-doped forsterite. European Journal of Mineralogy, 33, 113–138.

Koga, K., Hauri, E., Hirschmann, M., and Bell, D. (2003) Hydrogen concentration analyses using SIMS and FTIR: Comparison and calibration for nominally anhydrous minerals. Geochemistry, Geophysics, Geosystems, 4, 1–20.

Kumamoto, K.M., Warren, J.M., and Hauri, E.H. (2017) New SIMS reference materials for measuring water in upper mantle minerals. American Mineralogist, 102, 537–547.

Libowitzky, E., and Rossman, G.R. (1997) An IR absorption calibration for water in minerals. American Mineralogist, 82, 1111–1115.

Lloyd, A.S., Ferriss, E., Ruprecht, P., Hauri, E.H., Jicha, B.R., and Plank, T. (2016) An assessment of clinopyroxene as a recorder of magmatic water and magma ascent rate. Journal of Petrology, 57, 1865–1886.

Matveev, S., and Stachel, T. (2007) FTIR spectroscopy of OH in olivine: A new tool in kimberlite exploration. Geochimica et Cosmochimica Acta, 71, 5528–5543.

Mayerhöfer, T.G., Mutschke, H., and Popp, J. (2016) Employing Theories Far beyond Their Limits — The Case of the (Boguer-) Beer – Lambert Law, 1948–1955.

Mayerhöfer, Thomas G., Pahlow, S., and Popp, J. (2020) The Bouguer-Beer-Lambert Law: Shining Light on the Obscure. ChemPhysChem, 21, 2029-2046

Mosenfelder, J.L., and Rossman, G.R. (2013a) Analysis of hydrogen and fluorine in pyroxenes : I. Orthopyroxene. American Mineralogist, 98, 1042–1054.

Mosenfelder, J.L., and Rossman, G.R (2013b) Analysis of hydrogen and fluorine in pyroxenes: II. Clinopyroxene. American Mineralogist, 98, 1042–1054.

819 Mosenfelder, J.L., Voyer, M. Le, Rossman, G.R., Guan, Y., Bel, D.R., Asimow, P.D., and Eiler,
820 J.M. (2011) Analysis of hydrogen in olivine by SIMS: Evaluation of standards and protocol.
821 American Mineralogist, 96, 1725–1741.
822 Naif, S., Key, K., Constable, S., and Evans, R.L. (n.d.) Melt-rich channel observed at the
823 lithosphere–asthenosphere boundary, 10–13.
824 Newcombe, M.E., Plank, T., Barth, A., Asimow, P.D., and Hauri, E. (2020) Water-in-olivine
825 magma ascent chronometry: Every crystal is a clock. Journal of Volcanology and
826 Geothermal Research, 398, 106872.
827 O'Leary, J.A., Rossman, G.R., and Eiler, J.M. (2007) Hydrogen analysis in minerals by
828 continuous-flow mass spectrometry. American Mineralogist, 92, 1990–1997.
829 Padrón-Navarta, J.A., Hermann, J., and O'Neill, H.S.C. (2014) Site-specific hydrogen diffusion
830 rates in forsterite. Earth and Planetary Science Letters, 392, 100–112.
831 Paterson, M.S. (1982) The determination of hydroxyl by infrared adsorption in quartz, silicate
832 glasses and similar materials. Bulletin de Mineralogie, 105, 20–29.
833 Peslier, A.H. and Luhr, J.F. (2006) Hydrogen loss from olivines in mantle xenoliths from Simcoe
834 (USA) and Mexico: Mafic alkalic magma ascent rates and water budget of the sub-
835 continental lithosphere. Earth and Planetary Science Letters, 242, 302-319.
836 Peslier, A.H., Luhr, J.F., and Post, J. (2002) Low water contents in pyroxenes from spinel-
837 peridotites of the oxidized, sub-arc mantle wedge. Earth and Planetary Science Letters, 201,
838 69–86.
839 Portnyagin, M., Almeev, R., Matveev, S., and Holtz, F. (2008) Experimental evidence for rapid
840 water exchange between melt inclusions in olivine and host magma. Earth and Planetary
841 Science Letters, 272, 541–552.

Sarafian, E., Gaetani, G.A., Hauri, E.H., and Sarafian, A.R. (2017) Experimental constraints on the damp peridotite solidus and oceanic mantle potential temperature. Science, 355, 942–945.

Stephant, A., Garvie, L.A.J., Mane, P., Hervig, R. and Wadhwa, M. (2018) Terrestrial exposure of a fresh Martian meteorite causes rapid changes in hydrogen isotopes and water concentrations. Nature Scientific Reports 8, 12385.

Takei, H., and Kobayashi, T. (1974) Growth and properties of Mg2SiO4 single crystals. Journal of Crystal Growth, 23, 121–124.

Tollan, P.M.E., Smith, R., O'Neill, H.S.C., and Hermann, J. (2017) The responses of the four main substitution mechanisms of H in olivine to H2O activity at 1050 °C and 3 GPa. Progress in Earth and Planetary Science.

Le Voyer, M., Asimow, P.D., Mosenfelder, J.L., Guan, Y., Wallace, P., Schiano, P., Stolper, E.M., and Eiler, J.M. (2014) Zonation of H_2O and F concentrations around melt inclusions in olivines. Journal of Petrology, 55, 685–707.

Wade, J.A., Plank, T., Hauri, E.H., Kelley, K.A., Roggensack, K., and Zimmer, M. (2008) Prediction of magmatic water contents via measurement of H2O in clinopyroxene phenocrysts. Geology, 36, 799–802.

Wegdén, M., Kristiansson, P., Skogby, H., Auzelyte, V., Elfman, M., Malmqvist, K.G., Nilsson, C., Pallon, J., and Shariff, A. (2005) Hydrogen depth profiling by p-p scattering in nominally anhydrous minerals. Nuclear Instruments and Methods in Physics Research, Section B: Beam Interactions with Materials and Atoms, 231, 524–529.

Weis, F.A., Ros, L., Reichart, P., Skogby, H., Kristiansson, P., and Dollinger, G. (2018) Hydrogen concentration analysis in clinopyroxene using proton–proton scattering analysis.

865 Physics and Chemistry of Minerals, 45, 669–678.

866 Withers, A.C., Hirschmann, M.M., and Tenner, T.J. (2011) The effect of Fe on olivine H2O
867 storage capacity: Consequences for H_2O in the martian mantle. American Mineralogist, 96,
868 1039–1053.

869 Withers, A.C., Bureau, H., Raepsaet, C., and Hirschmann, M.M. (2012) Calibration of infrared
870 spectroscopy by elastic recoil detection analysis of H in synthetic olivine. Chemical
871 Geology, 334, 92–98.

872 Wu, C., and Zhen Yu, J. (2018) Evaluation of linear regression techniques for atmospheric
873 applications: The importance of appropriate weighting. Atmospheric Measurement
874 Techniques, 11, 1233–1250.

875 York, D. (1966) Least-squares fitting of a straight line. Canadian Journal of Physics, 44, 1079–
876 1086.

877 York, D. (1969) Least squares fitting of a straight line with correlated errors. Earth and
878 Planetary Science Letters, 5, 320–324.

879

880

881

882

883

884

885

886

887

888

889

890

Tables

Table 1 – Standards and Blanks used to calibrate and monitor drift in SIMS H2O measurements

Sample	Phase	H_2O Published ppm	Method	Suggested H_2O ppm (this study)
GRR1012	Olivine	220±20[a]	NRA	125±39‡*
KLV23	Olivine	140±20[a]	NRA	97±20‡*
ROM177	Olivine	125±20[b]	FTIR by Bell Calibration	88±8‡
ROM250-2	Olivine	183±30[b]	FTIR by Bell Calibration	80±12‡
ROM250-13	Olivine	254±40[b]	FTIR by Bell Calibration	141±20‡
CM58	Olivine	22[c]	SIMS calibrated with Bell NRA olivines	16±2‡
SynFo100	Synthetic Forsterite Olivine†	< 1[d]	FTIR	NA §
M475ol	Synthetic Olivine	2019±343[e]	ERDA	1965±343 ¶
M443ol	Synthetic Olivine	1106±184[e]	ERDA	1052±184 ¶
M437ol	Synthetic Olivine	925±176[e]	ERDA	871±176 ¶
M472ol	Synthetic Olivine	793±147[e]	ERDA	739±147 ¶
M449ol	Synthetic Olivine	769±129[e]	ERDA	715±129 ¶
A710ol	Synthetic Olivine	468±81[e]	ERDA	414±82 ¶
M469ol	Synthetic Olivine	283±50[e]	ERDA	229±51¶
ROM-273-OG2	Orthopyroxene	263±13[d,b,f]	FTIR	245±19**
KBH-1	Orthopyroxene	217±11[g]	Manometry	202±15**
India Enstatite	Orthopyroxene	141±7[d,h,f]	FTIR	131±10**
Suprasil 3001/3002	Synthetic SiO_2 Glass	1± ~1[i,j]	IR Laser absorption (946nm, 1064nm, 1319nm)	NA §

891 Table 1.

892 Notes: NRA: nuclear reaction analysis. ERDA: elastic recoil detection analysis. FTIR: Fourier
893 transform infrared spectroscopy. References for published values: [a]Bell et al., 2003; [b]Bell et al.,
894 2004; [c]Hauri unpublished; [d]Koga et al. 2003; [e]Withers et al. (2012); [f]Kumamoto et al. 2017;
895 [g]Bell et al. 1995; [h]Aubaud et al 2007; [i]Hereaus, 2019; [j]Hereaus, 2020. For revised
896 concentrations: * Heterogeneous Sample; ‡ Revised to the long-term average of samples
897 measured on the Carnegie 6F using the orthopyroxene calibration presented in this paper.; †
898 Synthetic Forsterite produced by Takei and Kobayashi, 1974; § near blank standard no change; ¶
899 subtracted ERDA blank of 54±10 (Withers et al., 2012); **Revised as discussed in text
900

901

902

Table 2 - Coefficients and R^2 Values for lines fit to calibration measurements

903

904

Calibration	Slope	Y-Intercept	R^2
June 2017 No Blank Correction[a]			
Opx no Blank	97±2	-10.8±5	0.998
Withers Olivine as Published	75±2.5	64±24	0.994
June 2017 Blank Corrected[b]			
Opx blank included	94±0.6	-4.4±0.3	0.9996
Withers Olivine	76±1.5	-3.4±0.3	0.993
Bell Olivine	156±20	-7.9±1.9	0.771
August 2016 Blank Corrected[c]			
Opx blank included	117±3	-2.7±0.5	0.9996
Bell Olivine	204±17	-4.7±1	0.993

Notes: [a]Calibration shown in Fig. 1; [b]Calibration shown in Fig. 2; [c]Calibration shown in Supplementary Fig. S1

905

906

907

908

909

910

911

912

This is the peer-reviewed, final accepted version for American Mineralogist, published by the Mineralogical Society of America.
The published version is subject to change. Cite as Authors (Year) Title. American Mineralogist, in press.
DOI: https://doi.org/10.2138/am-2022-8247. http://www.minsocam.org/

913

914

915

Table 3- Kumamoto et al. 2017 Orthopyroxene and Clinopyroxene concentration measured in this study.

	Sample	Measured August 2016 ppm	1σ	Measured June 2017 ppm	1σ	Published ppm	1σ	Revised ppm *	1σ
Orthopyroxene	109426-1	208	11	200	43	241	15	NA	NA
	116610-15	233	6	241	7	234	22	221	20
	116610-16	247	4	256	1	264	28	234	26
	116610-18	113	1	112	1	119	11	105	10
	116610-29	53	2	56	3	62	5	51	5
	116610-5	304	3	315	2	309	27	288	25
	117213-5	149	3	162	1	169	11	145	10
	117322-245	194	4	160	74	211	12	180*	10
	KH03-27	183	2	201	3	182	19	179	18
	KH03-4	220	2	225	1	216	14	207	13
Clinopyroxene	116610-14	283	4	225	17	356	48	254	33
	116610-15	333	4	271	6	441	61	302	34
	116610-16	371	2	309	4	490	66	340	34
	116610-18	155	2	123	12	199	27	139	19
	116610-5	381	5	284	10	544	79	332	54
	117213-5	243	4	174	7	315	40	202	38
	117322-242	119	1	77	0	127	16	94	23
	KH03-27	281	3	229	17	367	49	255	30
	KH03-4	287	5	241	8	427	59	264	26
	SC-J1	56	1	35	1	62	9	46	11
	SMC31139	7	2	0	0	5	0	3	4

916 Notes: Revised orthopyroxene concentrations are the averages of the values measured in the
917 August 2016 and June 2017 NanoSIMS session multiplied by a factor of 0.93 to account for
918 revisions to the orthopyroxene calibrations presented in this paper. Standard deviations have
919 been propagated from the published values. Concentrations for clinopyroxenes are derived from
920 the average of the Libowitsky and Rossman (1997) based clinopyroxene calibration (Fig. S5a)
921 and the calibration for basaltic glasses. The revised concentrations are the average of the values
922 measured in the August 2016 and June 2017 NanoSIMS session. These are within ~5% of the
923 concentrations that may be derived from the Kumamoto et al. (2017) supplementary data with
924 similar calibrations. *Concentration for orthopyroxene 117322-245 was determined from only
925 the August 2016 measurements due to the high uncertainty in the June 2017 measurements.

926
927

928

929 **Figure Captions**

930 **Figure 1.** Calibration lines for H_2O concentrations in olivine (blue) and orthopyroxene (green)
931 by the Carnegie Cameca NanoSIMS 50L in June 2017. The X-axis is the measured $^{16}O^{1}H/^{30}Si$
932 ion ratio multiplied by the wt% SiO_2 concentration of each standard; the Y-axis shows the
933 accepted H_2O concentration for each standard (concentrations and references given in Tables 1).
934 Inset shows the entire dataset, which is then expanded to magnify data for H_2O concentrations
935 lower than 600 ppm. Symbol shape distinguishes published H_2O concentrations by method of
936 analysis; symbol color distinguishes phase analyzed (olivine: blue; orthopyroxene: green;
937 Suprasil SiO_2 glass: grey). The star symbol represents the Withers et al. (2017) ERDA blank of
938 54 +/- 10 ppm. The Withers olivine calibration line is not fit through this data point yet the
939 determined Y-intercept agrees well with this value suggesting this blank should be subtracted
940 from the reference values. In contrast, the orthopyroxene calibration line passes through the
941 Suprasil blank demonstrating the precision of this calibration. The blue and green shaded regions
942 contain the regression and 95% confidence interval, using a weighted orthogonal-distance-
943 regression (WODR) to account for uncertainty in both the measured element ratios and the
944 known concentrations. Error bars represent 1 sigma uncertainties. Uncertainties in $^{16}O^{1}H/^{30}Si$ ion
945 ratio * SiO_2 are smaller than the symbols. Uncertainty in the calibration was assessed with
946 multiple regressions on bootstrapped samples consisting of 5000 random subsamples drawn with
947 replacement from the measurements (Efron, 1979). Confidence intervals were determined from
948 the histograms of possible H_2O concentrations in the bootstrapped calibration lines. Uncertainties
949 for India Enstatite and ROM273 (15 and 29 ppm respectively) used in this calibration differ from

published values (7 and 15 ppm) because we more thoroughly propagated errors from the FTIR calibration, which is solely dependent on KBH-1. Refer to Table 2 for slope, intercept and R^2.

Figure 2. The June 2017 NanoSIMS calibrations as in Figure 1 but modified such that the Withers et al. (2012) ERDA blank (54 +/- 10 ppm) has been subtracted from those sample's reference concentrations and all calibration lines have been fit to include Suprasil glass as a near-blank. The scale of the axes has been rescaled compared to figure 1 in order better show the details of each calibration. Also shown in light-green are olivine data and the resulting regression using olivines from Bell et al. (2003 and 2004). Dashed line represents the revised orthopyroxene calibration based on the manometry measurements of KBH-1 by Bell. et al. (1995), as discussed in the text. Refer to Table 2 for slope, intercept and R^2.

Figure 3. Comparison of $^{16}O^{1}H/^{30}Si$ ion ratio (multiplied by the wt% SiO_2 of each standard) and integrated IR absorbance (cm^{-2}) from the OH-stretching region (3000-3750 cm^{-1}). Ion ratios were measured on the Carnegie Cameca NanoSIMS 50L in June 2017. Blue diamonds are the olivines measured by Withers et al. (2012). The full range of these samples can be seen in the inset plot. The blue line and shading represent the best fit line and 68% confidence interval for all of the Withers et al. (2012) samples. The small red pentagons are olivines KLV23 and GRR1012, measured by Bell et al. (2003). The integrated absorbances for these samples include peaks indicative of hydrous non-olivine inclusions between 3650 and 3750 cm^{-1} (Mosenfelder et al., 2011). The 68% confidence interval for the best fit line (red) for these samples spans the full range of the other shaded regions depicted here and therefore has been omitted for visual clarity. The larger pink pentagons (Carnegie olivine) indicate samples which either do not have

973 significant IR peaks from hydrous non-olivine inclusions (ROM177, ROM250-13) or for which
974 spectra have been reintegrated to exclude OH-stretching bands above 3650 cm^{-1} (KLV23,
975 GRR1012). Integrated absorbances for ROM177 and ROM250-13 are as reported in
976 Mosenfelder et al. (2011). The Withers and Carnegie olivines plot along the same line within
977 uncertainty. The best fit line for the combined samples is Y = 623±13 * X + 117±39. Uncertainty
978 on integrated absorbance is assumed to be 10% using the same assumption of Withers et al.
979 (2012). High $^{16}O^{1}H/^{30}Si$ measurements of KLV23 have been excluded from the data points
980 plotted here.
981
982 **Figure 4.** Comparison of published H_2O concentrations in the orthopyroxene standards in
983 Kumamoto et al. (2017) to the SIMS measurements at Carnegie during August 2016 (green
984 circles) and June 2017 (green squares). The two samples (SMNH ID:109426-1 and 117322-245)
985 with measured concentrations that differ from the published values by more than -10% are
986 shown in darker green and labeled. Data are calibrated using the Carnegie orthopyroxene
987 standards: KBH-1 (Bell et al., 1995); India enstatite (Koga et al., 2003; Aubaud et al., 2007;
988 Kumamoto et al. 2017); ROM 273 (Koga et al., 2003; Bell et al., 2004; Kumamoto et al., 2017)
989 which are shown as blue triangles and diamonds for the 2016 and 2017 SIMS sessions
990 respectively. Data have been corrected for instrumental drift using KBH-1 measured on both the
991 standard mount and sample mount.
992
993 **Figure 5.** Partition coefficients (K_d) for H_2O between olivine and melt. a) K_ds published by Koga
994 et al., 2003 (green); Aubaud et al., 2004 (orange); Hauri et al., 2006 (blue); and Newcombe et al.,
995 2020 (purple). b) K_ds recalculated to be consistent with the Withers et al. (2012) calibration for

H_2O in olivine using the revised orthopyroxene calibration, as described in the text. Recalculated Kds are only shown for those studies that measured both orthopyroxene and olivine standards. Concentrations of H_2O in the melt phase were not adjusted. Symbols distinguish between experimental studies (circles) and measurements of melt-inclusion and olivine host pairs (triangles). Shaded regions represent 1σ (65% CI) distributions for K_d coefficients: Published experimental studies average 0.00153 +0.00062/ -0.00034 (orange); melt inclusion studies average 0.00083 +/-0.00025 (purple); and revised K_d from the combined experimental and melt-inclusion studies average 0.0009 +0.0003/ -0.0002 (blue).

Figures

Fig. 1

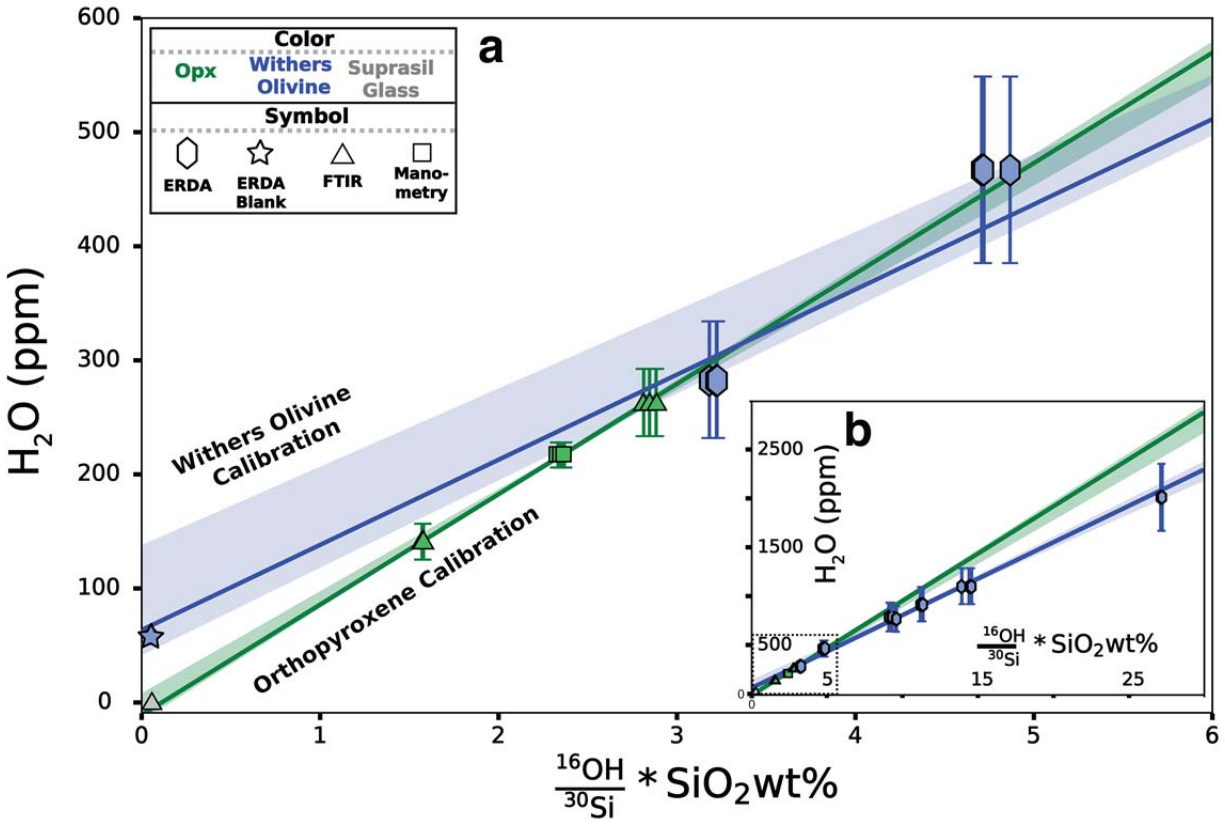

This is the peer-reviewed, final accepted version for American Mineralogist, published by the Mineralogical Society of America.
The published version is subject to change. Cite as Authors (Year) Title. American Mineralogist, in press.
DOI: https://doi.org/10.2138/am-2022-8247. http://www.minsocam.org/

1008 **Fig. 2**

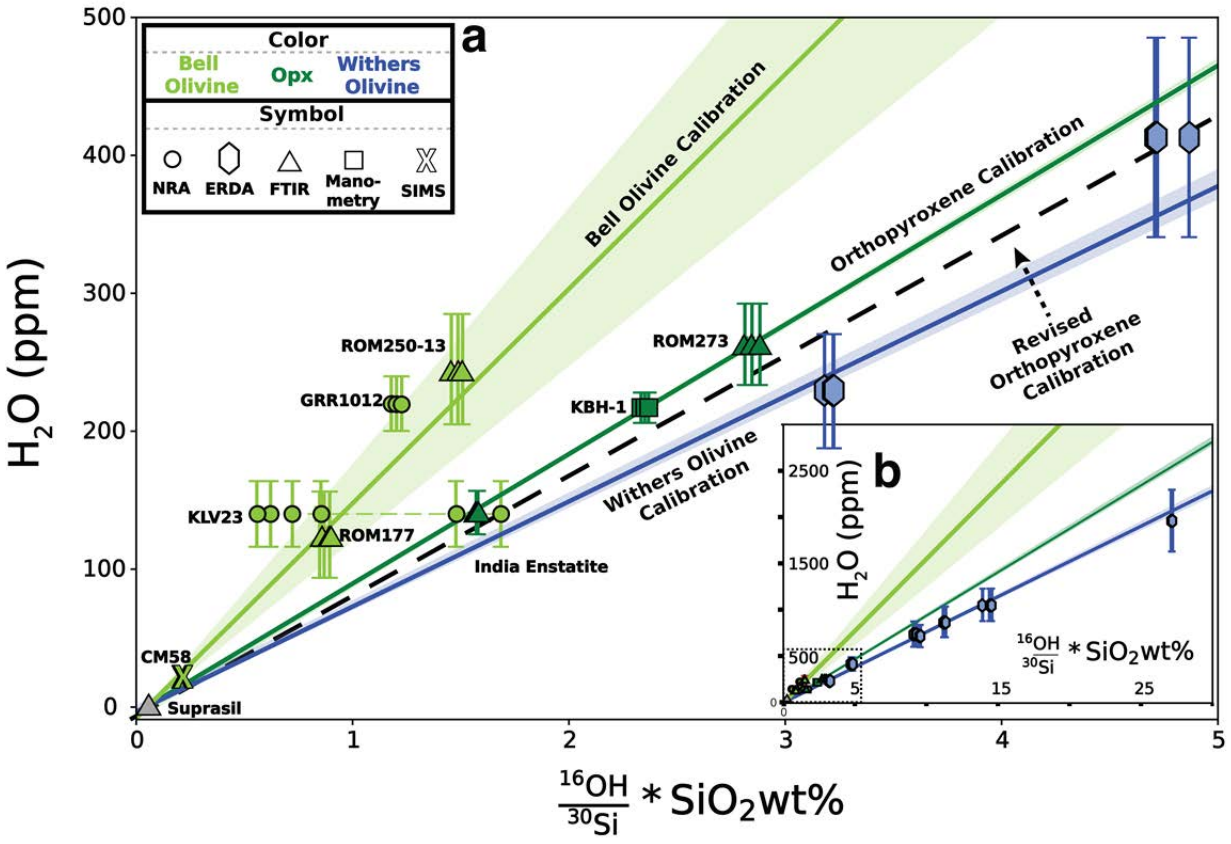

1009

1010

1011

1012

1013

1014

1015

1016

1017

1018

1019

This is the peer-reviewed, final accepted version for American Mineralogist, published by the Mineralogical Society of America.
The published version is subject to change. Cite as Authors (Year) Title. American Mineralogist, in press.
DOI: https://doi.org/10.2138/am-2022-8247. http://www.minsocam.org/

1020 **Fig. 3**

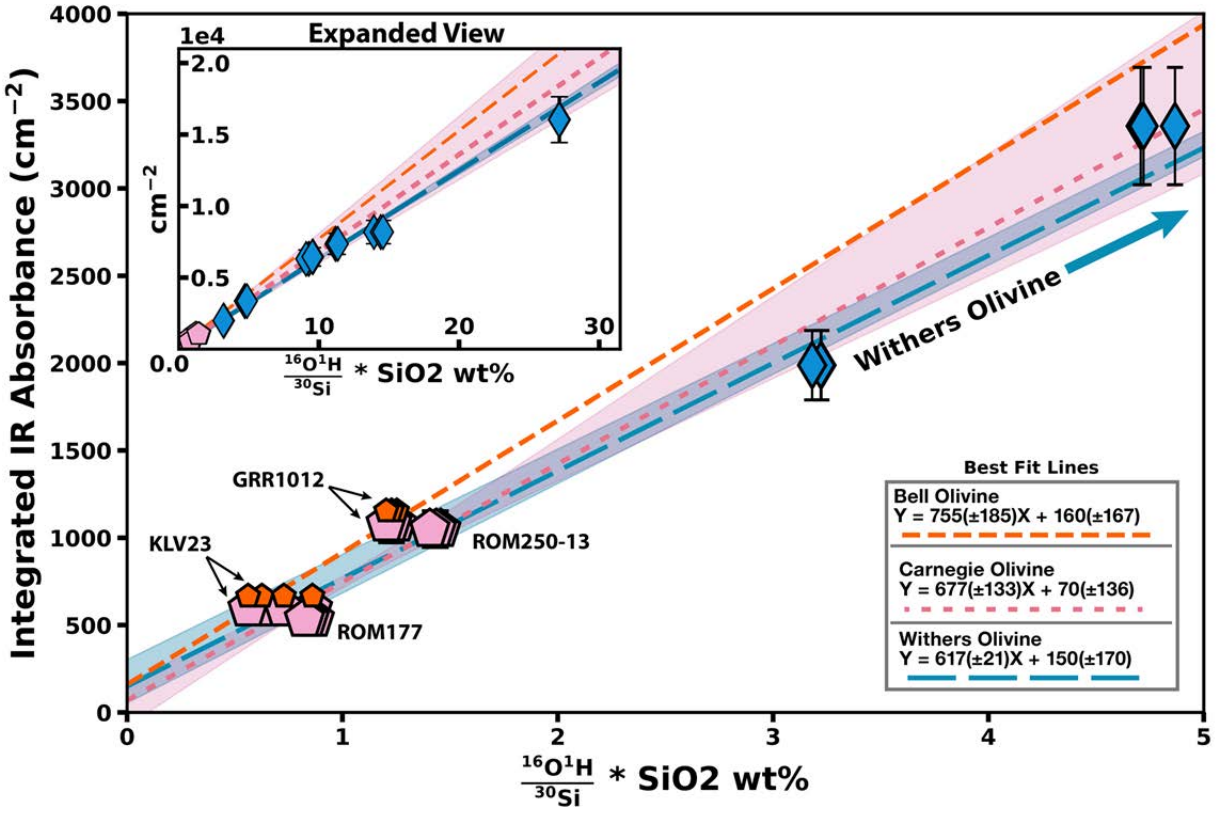

1021

1022

1023

1024

1025

1026

1027

1028

1029

1030

1031

1032 **Fig. 4**

1033

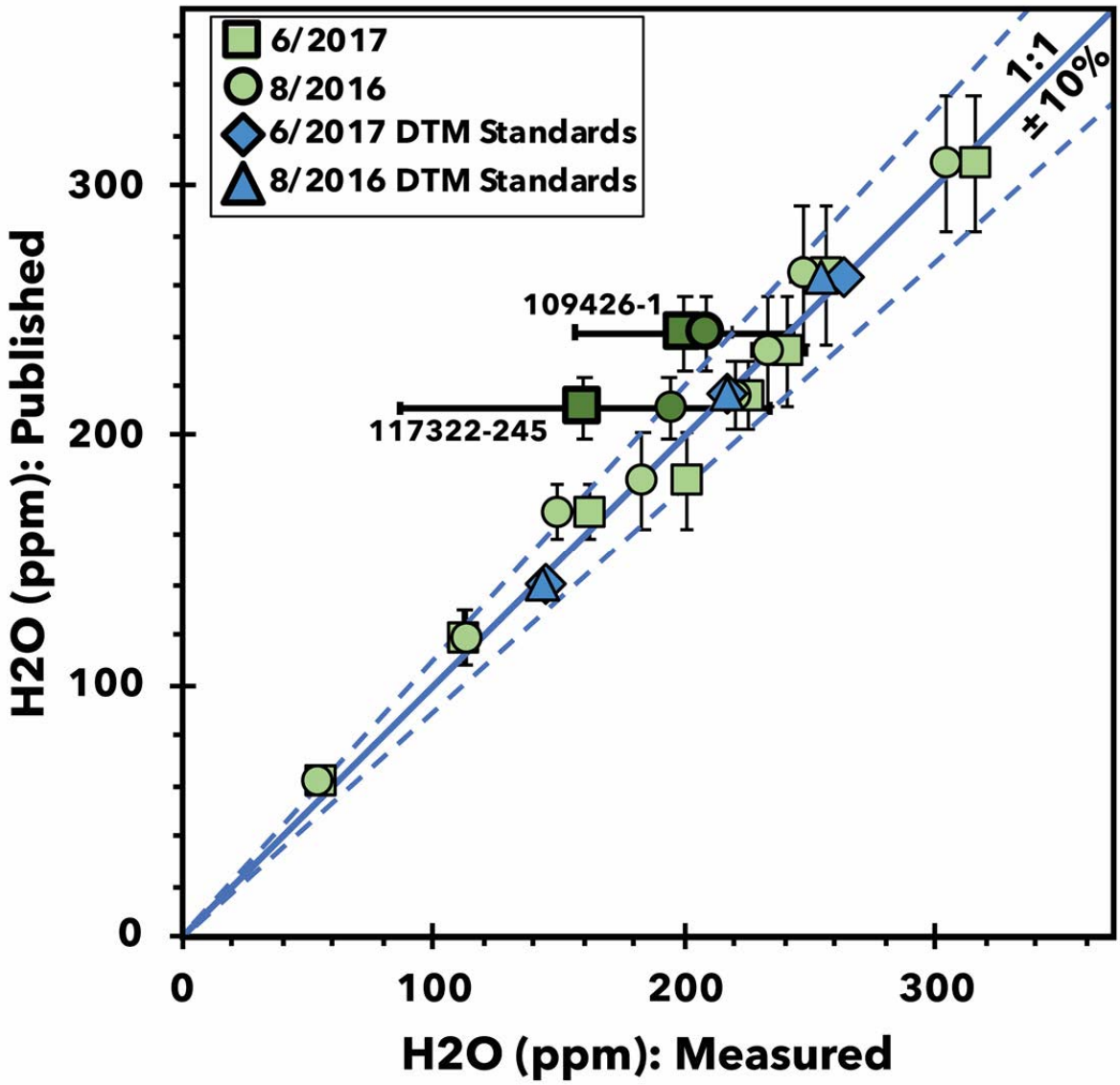

1034

This is the peer-reviewed, final accepted version for American Mineralogist, published by the Mineralogical Society of America.
The published version is subject to change. Cite as Authors (Year) Title. American Mineralogist, in press.
DOI: https://doi.org/10.2138/am-2022-8247. http://www.minsocam.org/

1035 **Fig. 5**

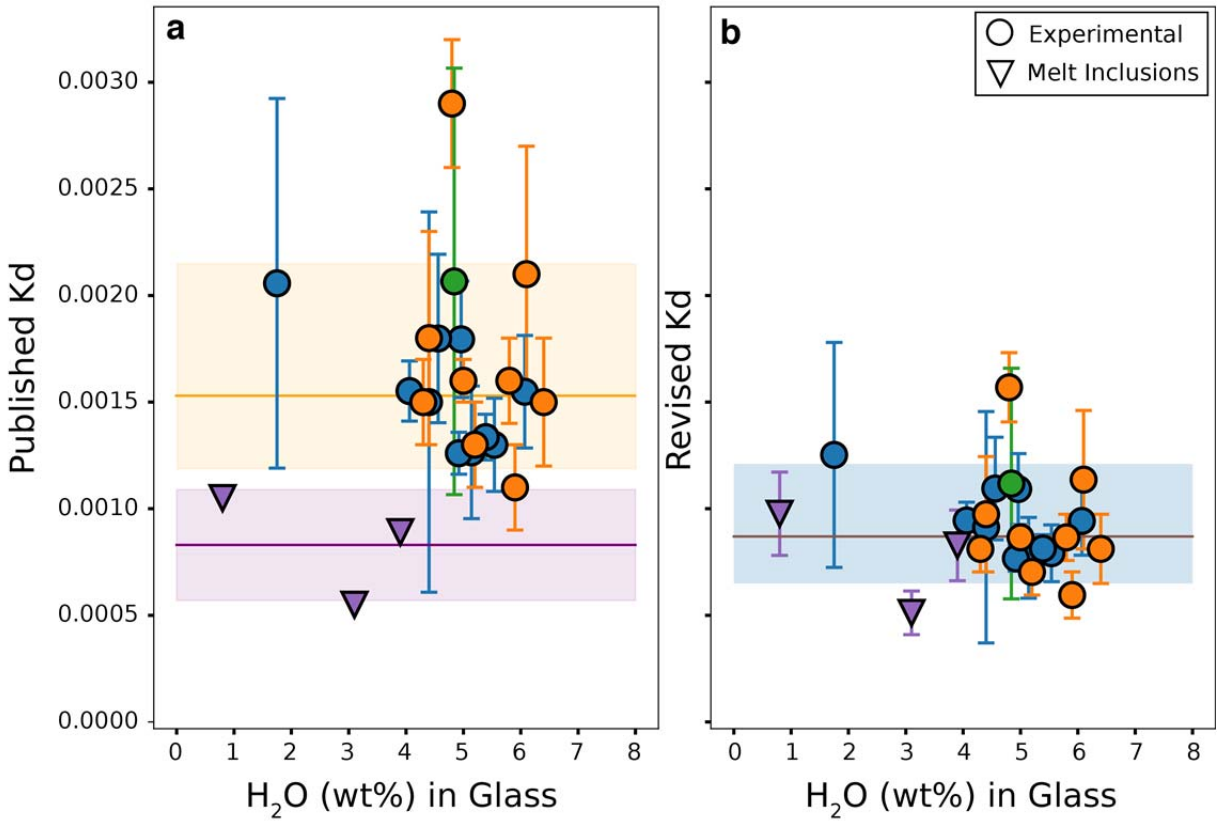

1036

1037